

## Photoelectric Cross Sections in the keV Range\*

H. BRYSK† AND C. D. ZERBY‡

*Union Carbide Corporation, Materials Systems Division, White Plains, New York*

(Received 21 February 1968)

Photoelectric cross sections have been computed using bound-state wave functions and potentials from a relativistic Dirac-Slater self-consistent-field program and numerical integration for the continuum wave functions and the matrix elements. Results for aluminum in the range 1–150 keV and for uranium in the range 80–150 keV are compared with existing experimental and theoretical data, with particular emphasis on the angular distributions.

### I. INTRODUCTION

THE theoretical literature on the photoelectric effect is abundant, reflecting at first progressively more sophisticated or more laboriously intricate analytical expressions, later, increasingly more complex numerical calculations as the computer art advanced. The computations have now progressed to the utilization of the output of central-field atomic-structure calculations for the bound-state electron wave functions and the potential, and numerical integration for the free-electron wave functions and the matrix elements. This has been done nonrelativistically<sup>1</sup> with a Hartree-Fock-Slater self-consistent field<sup>2</sup> and relativistically<sup>3</sup> with variants of the Thomas-Fermi potential. These very recent papers cover the historical perspective<sup>3</sup> and the import of the central-field approximation (i.e., neglect of electron-electron correlation).<sup>1</sup>

The present calculation is relativistic and hence not limited to the dipole approximation. It uses for the bound-state wave functions and the potential the output (on tape) of a self-consistent-field calculation<sup>4</sup> in the Dirac relativistic version with the Slater density approximation for exchange (modified at large radii to a singly ionized point atom—but that occurs beyond the atomic region of consequence for the photoelectric effect). The Gill form of Runge-Kutta integration<sup>5</sup> is used to obtain the free-electron wave functions and the matrix elements. The free-electron wave functions are normalized by matching to the WKB solution.<sup>6</sup> The derivation of the cross section will not be given here, since it agrees substantially with that given by Rakavy and Ron,<sup>3</sup> differing only in the exploitation of some specialized results of Racah algebra for computational

advantage. Full analytical details can be found in a technical report<sup>7</sup> which also includes a complete description of the program.

For a given element and incident photon energy, the program produces the differential and the integrated cross section for each subshell and the total atomic cross section. The bulk of data generated for different elements and energies poses an information-presentation problem. The present paper concentrates on an intensive look at sample results—explicitly, the aluminum cross sections from 1 to 150 keV and uranium cross sections from 80 to 150 keV—with emphasis on the angular distributions. The perspective is largely complementary to that of the most recent publications.<sup>1,3</sup> The program is in production status on the CDC 6600 computer at the Air Force Weapons Laboratory (Kirtland Air Force Base, Albuquerque, N.M.), and there are plans for issuance of an extensive tabulation of cross sections as a function of atomic number and photon energy.

### II. TOTAL CROSS SECTIONS

Table I gives a comparison of some of our aluminum results with those of the most precise previous computations. At energies below 10 keV our relativistic self-consistent-field calculations agree closely with Manson and Cooper's<sup>4</sup> nonrelativistic self-consistent-field calculations (illustrated at 10 keV in Table I). This is expected, since the potentials are quite similar. At higher energies there is a deviation. This is again expected, since the nonrelativistic treatment becomes less satisfactory as the energy increases. Restricting our calculations to photon dipole terms, as happens nonrelativistically, actually leads to a discrepancy in the opposite direction. The Rakavy and Ron calculations,<sup>3</sup> using a Thomas-Fermi potential, give lower cross sections than ours for all shells, with the largest discrepancy for the outer shells. This can be understood on the basis that the inaccuracies of the Thomas-Fermi potential for light elements lead to outer shells that lie too far from the nucleus.

For uranium, Table II shows that our results and those of Rakavy and Ron agree quite well. This is not

\* Work performed under Contract No. DA-49-146-XZ-511 with the Defense Atomic Support Agency, monitored by the Air Force Weapons Laboratory.

† Present address: New York Regional Computer Center, Union Carbide Research Institute, P.O. Box 278, Tarrytown, N.Y.

‡ Present address: Union Carbide Corporation, Electronics Division, Santa Monica, Calif.

<sup>1</sup> S. T. Manson and J. W. Cooper, *Phys. Rev.* **165**, 126 (1968).

<sup>2</sup> F. Herman and S. Skillman, *Atomic Structure Calculations* (Prentice-Hall, Inc., Englewood Cliffs, N.J., 1963).

<sup>3</sup> G. Rakavy and A. Ron, *Phys. Rev.* **159**, 50 (1967).

<sup>4</sup> D. Liberman, J. T. Waber, and Don T. Cromer, *Phys. Rev.* **137**, A27 (1965).

<sup>5</sup> S. Gill, *Proc. Cambridge Phil. Soc.* **47**, 96 (1951).

<sup>6</sup> C. D. Zerby, Electromagnetic Production of Pion Pairs, Oak Ridge National Laboratory Report No. ORNL-3033, 1961 (unpublished).

<sup>7</sup> H. Brysk and C. D. Zerby, Low-Energy Photoelectric Cross Section Calculations, Union Carbide Corporation Report No. UCC/DSSD-299, 1967 (unpublished).

TABLE I. Aluminum cross sections (in barns) by subshell (comparison of Brysk-Zerby, Rakavy-Ron, Manson-Cooper, and Schmickley-Pratt results) for 10-keV and 30-keV photons.

	<i>K</i>	<i>L<sub>I</sub></i>	<i>L<sub>II</sub></i>	<i>L<sub>III</sub></i>	<i>L<sub>II</sub>+L<sub>III</sub></i>	<i>K+L</i>	Total
10 keV							
BZ	1066	67.6	2.63	5.07	7.70	1141	1146
RR	1036	60.8	2.05	3.93	5.98	1103	
MC	1064	67.1			7.6	1139	
SP	1020	68.6	2.61	4.76	7.37	1096	1100
30 keV							
BZ	36.5	2.49	0.0355	0.0665	0.102	39.1	39.3
RR	35.2	2.21	0.0274	0.0516	0.079	37.5	
MC	36.2	2.22			0.079	38.5	
SP	35.1	2.49	0.0349	0.0625	0.097	37.7	37.8

surprising, since the Thomas-Fermi potential is reasonably accurate for heavy elements.

In Tables I and II, the calculations of Schmickley and Pratt<sup>8</sup> are also given for comparison. They upgrade previously obtained cross-section calculations by re-

scaling the matrix elements by the ratio of photoelectron normalization factors squared [(new wave functions)/(old)], thus obtaining approximate results for the same potential that we use.<sup>4</sup> The agreement is very good for uranium, reflecting the fact that the Rakavy-Ron values need essentially no correction (in fact, the Rakavy-Ron results fit better without the correction). On the other hand, the pure-Coulomb results<sup>9</sup> are appreciably off. For aluminum, the Schmickley-Pratt values are closer to ours than to Rakavy-Ron (except for the *K* shell).

Our total photoelectric cross sections for aluminum are given in Table III, together with the corresponding entries from the LRL compilation.<sup>10</sup> The agreement is very good throughout, the spread never exceeding 6% and mostly remaining well below that. In fairness, it must be conceded that this does not represent an unbiased comparison of theory and experiment, since the authors of the compilation eke out fragmentary experimental data with systematics and available theory. The contributions of the individual subshells to the cross section are plotted in Fig. 1. For convenience, the calculated values have been divided by the simplest approximation for the *K*-shell cross section<sup>11</sup>:

$$\sigma_0 = \left(\frac{4}{3}\pi\right) r_e^2 \alpha^4 Z^5 (2m_e c^2 / q)^{7/2}, \quad (1)$$

where  $r_e$  is the classical electron radius,  $\alpha$  the fine-structure constant,  $Z$  the atomic number,  $m_e c^2$  the electron rest energy, and  $q$  the photon energy.

### III. DIFFERENTIAL CROSS SECTIONS

Experimental results for the angular distribution of photoelectrons are scarce. They are limited to a few energies at which high-intensity nuclear  $\gamma$ -ray sources are available, mostly with uranium as target. As a typical example, Fig. 2 displays a comparison of the calculated *L*-shell differential cross section of uranium

<sup>9</sup> W. R. Alling and W. R. Johnson, Phys. Rev. **139**, A1050 (1965).

<sup>10</sup> W. H. McMaster, N. Kerr Del Grande, J. H. Mallett, N. E. Scofield, R. Cahill, and J. H. Hubbell, University of California Radiation Laboratory Report No. UCRL-50174, 1967 (unpublished).

<sup>11</sup> W. Heitler, *The Quantum Theory of Radiation* (Oxford University Press, London, 1954).

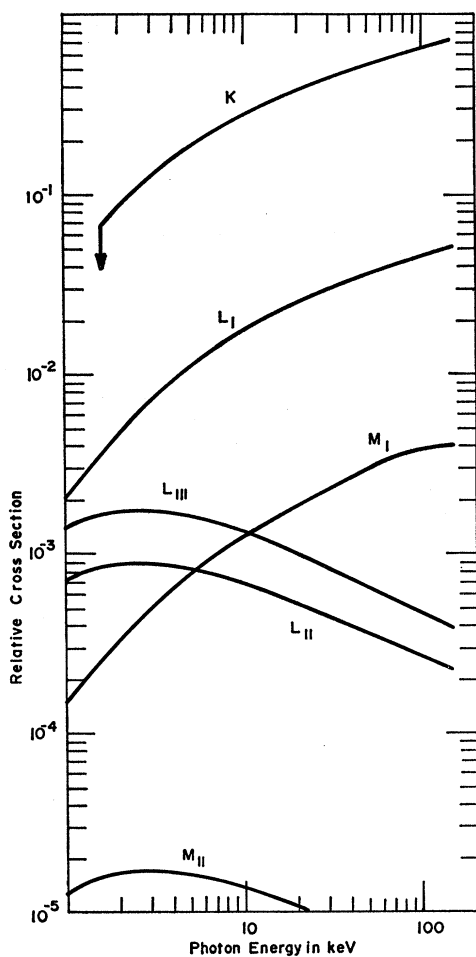


FIG. 1. Aluminum cross section by subshells in units of Heitler *K*-shell cross section.

<sup>8</sup> R. D. Schmickley and R. H. Pratt, Phys. Rev. **164**, 104 (1967).

TABLE II. Uranium cross sections (in barns) by subshell (comparison of Brysk-Zerby, Rakavy-Ron, Schmickley-Pratt and Alling-Johnson results) for 103-keV photons.

	$L_I$	$L_{II}$	$L_{III}$	$M_I$	$M_{II}$	$M_{III}$	$M_{IV}$	$M_V$	$M$
BZ	195.1	135.7	112.0	44.70	30.31	26.87	2.870	2.835	107.6
RR	194.9	135.8	112.2	44.48	30.17	26.76	2.88	2.843	107.1
SP	194.0	134.0	111.0						106.0
AJ	219.0	162.6	139.4						
	$N_I$	$N_{II}$	$N_{III}$	$N_{IV}$	$N_V$	$N_{VI}$	$N_{VII}$		
BZ	12.19	8.00	7.12	0.838	0.825	0.0152	0.0158		
RR	12.11	7.95	7.10	0.839	0.827	0.0152	0.0156		
	$O_I$	$O_{II}$	$O_{III}$	$O_{IV}$	$O_V$				
BZ	3.18	1.96	1.72	0.174	0.171				
RR	3.10	1.90	1.64	0.160	0.154				

for 103-keV photons with the uncorrected experimental results of Sujkowski.<sup>12</sup> Since the measurements are relative, both curves have been normalized to a peak value of unity. The agreement is satisfactory, since corrections of the data for finite solid angles and for scattering effects can easily account for the discrepancies. In fact, Sujkowski assigns corrections to his 279-keV results that exceed these discrepancies, except in the backward direction where scattering should be more intense at the lower energy.

The difficulty of handling the mass of numbers generated in computations of the differential cross sections leaves consideration of analytic approximations and systematic trends pertinent even when exact numerical results are available. Comparison with the accurate calculations indicated that the approximate expressions gave differential cross sections incorrect in magnitude but of roughly the right shape for light elements. The systematic patterns of the exact differential cross sections obtained for different shells emerged more clearly on abstracting the shape of the angular distribution from its scale. Hereafter, the term "angular distribution" will be used to denote the differential cross section divided by its peak value. This particular normalization is the most useful for comparisons with experiment.

Sauter<sup>13</sup> carried out a Sommerfeld-type nonrelativistic approximate calculation for the  $K$ - and  $L$ -shell photoelectron wave functions. Keeping terms of lowest order in  $(\alpha Z/\text{velocity})$  and neglecting  $q$  compared with  $m_e c^2$ , he then obtained for the  $K$  shell an angular distribution (apart from normalization)

$$I(\theta) = \sin^2\theta (E - k \cos\theta)^{-4}, \quad (2)$$

where  $E$  is the electron energy in  $m_e c^2$  units and  $k$  is the electron momentum in  $m_e c$  units. Equation (2) differs from Sauter's result by specialization to the unpolarized case and substitution of  $(k/E)$  for the velocity. Subsequently, he demonstrated<sup>14</sup> that the analogous Dirac treatment reduced in lowest order to Eq. (2) in both the high- and low-energy limits

(though differences appeared in the next order). To the next order in the high-energy relativistic limit, he obtained

$$I(\theta) = \sin^2\theta (E - k \cos\theta)^{-4} \times [1 - \frac{1}{2}(E-1)(2-E)(E - k \cos\theta)]. \quad (3)$$

The second term in the bracket is fairly small at 150 keV and essentially negligible below half this energy. Higher-order calculations exist<sup>15</sup> but are not relevant till much higher energies. If Sauter's nonrelativistic calculation<sup>13</sup> is carried forward to lowest order for the  $L_I$  subshell, the angular distribution obtained is again Eq. (2). The analogous calculation for the  $p$  electrons (with the  $L_{II}$  and  $L_{III}$  subshells combined, since the calculation is nonrelativistic) yields

$$I(\theta) = (E - k \cos\theta)^{-2} + kE^{-2}(E+1)(E - k \cos\theta)^{-5}(E \cos\theta - k) \sin^2\theta. \quad (4)$$

Table IV presents the angular distributions for 10-keV photons on aluminum. The agreement between the  $K$ -shell angular distribution and Sauter's [Eq. (2)] is fairly good. This also holds true at lower photon energies, down to the edge where the computed shape

TABLE III. Photoelectric cross sections for aluminum (in barns).

Energy (keV)	Calculated	LRL compilation
1.00	$5.301 \times 10^4$	$5.128 \times 10^4$
1.55	$1.641 \times 10^4$	$1.545 \times 10^4$
1.56	$1.789 \times 10^5$	$1.873 \times 10^5$
2.00	$1.012 \times 10^5$	$1.015 \times 10^5$
3.00	$3.524 \times 10^4$	$3.548 \times 10^4$
5.00	$8.611 \times 10^3$	$8.703 \times 10^3$
10.00	$1.146 \times 10^3$	$1.149 \times 10^3$
20.00	$1.391 \times 10^2$	$1.372 \times 10^2$
30.00	$3.931 \times 10^1$	$3.858 \times 10^1$
40.00	$1.582 \times 10^1$	$1.541 \times 10^1$
60.00	$4.341 \times 10^0$	$4.234 \times 10^0$
80.00	$1.729 \times 10^0$	$1.692 \times 10^0$
100.00	$8.417 \times 10^{-1}$	$8.323 \times 10^{-1}$
150.00	$2.255 \times 10^{-1}$	$2.312 \times 10^{-1}$

<sup>12</sup> Z. Sujkowski, Arkiv Fysik **20**, 269 (1961).<sup>13</sup> F. Sauter, Ann. Physik **9**, 217 (1931).<sup>14</sup> F. Sauter, Ann. Physik **11**, 454 (1931).<sup>15</sup> M. Gavrila, Phys. Rev. **113**, 514 (1959).

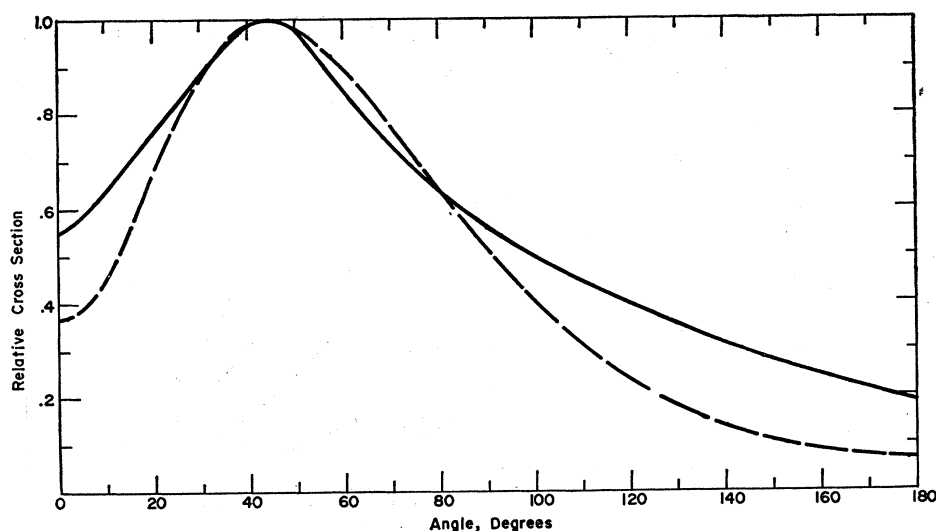


FIG. 2. Angular distribution of photoelectrons from the  $L$  shell of uranium for 103-keV photons. The uncorrected experimental curve (solid line) and the theoretical curve (dashed line) have both been normalized to unity at their peak.

closely agrees with what Sauter's formula would give for 9-keV electrons. The angular distributions for all  $s$  electrons ( $K$  shell,  $L_I$  and  $M_I$  subshells) are just about identical. This holds true down to the edge. Similarly, the angular distributions for all  $p$  electrons ( $L_{II}$ ,  $L_{III}$ , and  $M_{II}$  subshells) are closely alike, at 10 keV and also below. The Sauter-derived expression [Eq. (4)] is in fair agreement with the  $p$ -electron distributions at 10 keV except in the forward direction. As the photon energy is decreased, this agreement deteriorates quickly; as it is increased, the agreement improves.

The corresponding results for aluminum at 150 keV are given in Table V. Again, the  $s$ -electron angular distributions are nearly identical. The calculated data show fairly good agreement with the lower-order Sauter expression [Eq. (2)] and excellent agreement with the higher-order expression [Eq. (3)]. The  $p$ -electron

distributions are much more crudely similar, differing in the forward and backward directions. The combined  $L_{II}+L_{III}$  shape is reasonably like the Sauter-derived expression [Eq. (4)], as is  $M_{II}$  except in the tail. Comparisons at energies between 10 and 150 keV yield intermediate results as to agreement.

Figure 3 displays the variation of the  $K$ -shell angular distribution in aluminum with photon energy, from the edge to 150 keV. The angular distributions for the  $L_I$  and  $M_I$  subshells are indistinguishable from the data shown in Fig. 3. The corresponding curves for the  $L_{III}$  subshell, the  $p$ -electron subshell of largest cross section, are given in Fig. 4. The  $L_{II}$  and  $M_{II}$  angular distributions are quite similar, differing mainly at the upper end of the energy range, where there is less of a dip forward of the peak. In both figures, the location of the peak moves to the forward direction with increasing energy.

TABLE IV. Angular distribution of photoelectrons from 10-keV photons on aluminum by subshell. Equations (2) and (4) are Sauter approximations for  $s$  and  $p$  states, respectively.

$\theta$	$K$	$L_{II}$	$M_I$	Eq. (2)	$L_{II}$	$L_{III}$	$M_{II}$	Eq. (4)
0	0.0001	0.0000	0.0000	0.0000	0.8740	0.8619	0.8622	0.9617
10	0.0560	0.0569	0.0569	0.0606	0.8914	0.8803	0.8812	0.9706
20	0.2092	0.2125	0.2126	0.2252	0.9341	0.9257	0.9277	0.9896
30	0.4215	0.4274	0.4276	0.4491	0.9787	0.9741	0.9763	0.9999
40	0.6439	0.6510	0.6517	0.6767	0.9999	0.9994	0.9999	0.9840
50	0.8313	0.8378	0.8387	0.8602	0.9826	0.9854	0.9826	0.9338
60	0.9538	0.9578	0.9584	0.9704	0.9256	0.9311	0.9241	0.8543
70	0.9998	0.9999	0.9999	0.9996	0.8405	0.8475	0.8371	0.7590
80	0.9737	0.9700	0.9693	0.9566	0.7436	0.7511	0.7392	0.6633
90	0.8903	0.8835	0.8823	0.8599	0.6502	0.6573	0.6461	0.5795
100	0.7685	0.7598	0.7585	0.7303	0.5702	0.5764	0.5676	0.5145
110	0.6270	0.6178	0.6168	0.5871	0.5081	0.5130	0.5075	0.4697
120	0.4817	0.4732	0.4724	0.4451	0.4641	0.4675	0.4647	0.4430
130	0.3448	0.3379	0.3373	0.3152	0.4354	0.4374	0.4358	0.4304
140	0.2252	0.2202	0.2196	0.2040	0.4186	0.4192	0.4166	0.4273
150	0.1283	0.1252	0.1248	0.1154	0.4098	0.4092	0.4038	0.4294
160	0.0575	0.0560	0.0557	0.0514	0.4059	0.4044	0.3955	0.4333
170	0.0145	0.0141	0.0140	0.0129	0.4045	0.4024	0.3906	0.4366
180	0.0001	0.0000	0.0001	0.0000	0.4042	0.4019	0.3890	0.4378

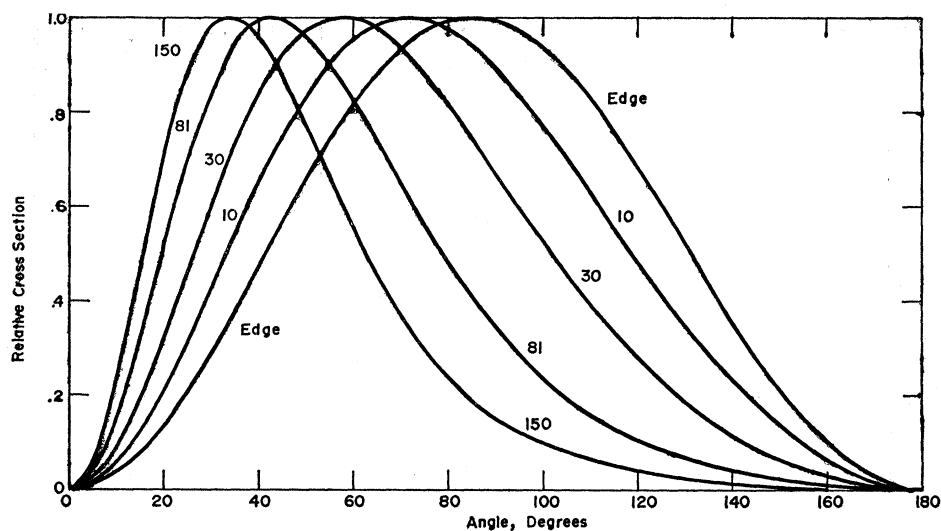


FIG. 3. Angular distribution of photoelectrons from the  $K$  shell of aluminum for various incident photon energies (in keV).

TABLE V. Angular distribution of photoelectrons from 150-keV photons on aluminum by subshell. Equations (2) and (4) are Sauter approximations for  $s$  and  $p$  states, respectively; Eq. (3) is Sauter's higher-order result for the  $K$  shell.

$\theta$	$K$	$L_I$	$M_I$	Eq. (2)	Eq. (3)	$L_{II}$	$L_{III}$	$L_{II}+L_{III}$	$M_{II}$	Eq. (4)
0	0.0000	0.0000	0.0000	0.0000	0.0000	0.9735	0.7586	0.8618	0.8921	0.8879
10	0.2426	0.2427	0.2424	0.2437	0.2471	0.9968	0.8684	0.9367	0.9579	0.9561
20	0.7086	0.7088	0.7081	0.7065	0.7135	0.9610	0.9987	0.9987	0.9918	0.9928
30	0.9807	0.9809	0.9806	0.9779	0.9812	0.7652	0.9006	0.8576	0.8152	0.8335
40	0.9527	0.9521	0.9523	0.9582	0.9528	0.5008	0.6348	0.5882	0.5278	0.5705
50	0.7638	0.7621	0.7617	0.7752	0.7623	0.2924	0.3862	0.3526	0.2993	0.3441
60	0.5501	0.5481	0.5472	0.5625	0.5459	0.1670	0.2286	0.2061	0.1707	0.2006
70	0.3711	0.3697	0.3693	0.3840	0.3672	0.0989	0.1424	0.1262	0.1047	0.1238
80	0.2406	0.2399	0.2401	0.2534	0.2385	0.0647	0.0961	0.0843	0.0688	0.0861
90	0.1534	0.1527	0.1528	0.1641	0.1519	0.0490	0.0715	0.0631	0.0501	0.0682
100	0.0970	0.0962	0.0958	0.1049	0.0955	0.0422	0.0582	0.0524	0.0430	0.0593
110	0.0602	0.0597	0.0595	0.0662	0.0593	0.0396	0.0508	0.0468	0.0419	0.0544
120	0.0365	0.0363	0.0365	0.0410	0.0361	0.0382	0.0465	0.0437	0.0408	0.0513
130	0.0216	0.0215	0.0217	0.0246	0.0214	0.0361	0.0439	0.0413	0.0367	0.0491
140	0.0123	0.0121	0.0120	0.0140	0.0120	0.0340	0.0418	0.0392	0.0330	0.0474
150	0.0063	0.0062	0.0061	0.0072	0.0061	0.0348	0.0388	0.0377	0.0364	0.0461
160	0.0026	0.0026	0.0026	0.0030	0.0025	0.0394	0.0351	0.0375	0.0518	0.0452
170	0.0006	0.0006	0.0009	0.0007	0.0006	0.0454	0.0321	0.0382	0.0748	0.0447
180	0.0000	0.0000	0.0006	0.0000	0.0000	0.0483	0.0309	0.0387	0.0866	0.0445

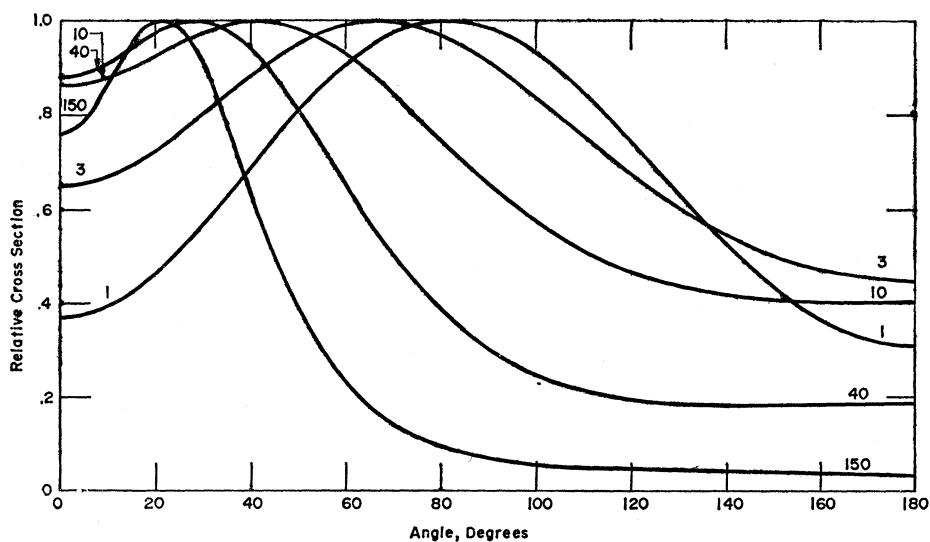


FIG. 4. Angular distribution of photoelectrons from the  $L_{III}$  subshell of aluminum for various incident photon energies (in keV).

TABLE VI. Angular distribution of photoelectrons from 81-keV photons on uranium by subshell (*s* states). Electron kinetic energies are about 59 keV for  $L_I$ , 75 keV for  $M_I$ , 80 or 81 keV for the others; for comparison, 103-keV photons on  $L_I$  yield 81-keV electrons (next-to-last column). Last column is Sauter approximation.

$\theta$	$L_I$	$M_I$	$N_I$	$O_I$	$P_I$	$Q_I$	103 $L_I$	Eq. (2)
0	0.0157	0.0183	0.0195	0.0197	0.0196	0.0184	0.0166	0.0000
10	0.0688	0.0756	0.0781	0.0788	0.0789	0.0778	0.0817	0.1605
20	0.2115	0.2310	0.2373	0.2393	0.2399	0.2394	0.2564	0.5216
30	0.4069	0.4446	0.4552	0.4587	0.4596	0.4598	0.4902	0.8482
40	0.6161	0.6675	0.6804	0.6840	0.6849	0.6852	0.7230	0.9944
50	0.8030	0.8533	0.8930	0.8671	0.8676	0.8677	0.9008	0.9596
60	0.9364	0.9684	0.9741	0.9754	0.9756	0.9756	0.9906	0.8177
70	0.9971	0.9997	0.9982	0.9978	0.9978	0.9978	0.9881	0.6419
80	0.9830	0.9555	0.9471	0.9445	0.9438	0.9437	0.9127	0.4768
90	0.9073	0.8569	0.8436	0.8392	0.8379	0.8376	0.7931	0.3407
100	0.7902	0.7276	0.7122	0.7077	0.7063	0.7060	0.6555	0.2361
110	0.6521	0.5880	0.5730	0.5692	0.5681	0.5678	0.5185	0.1591
120	0.5105	0.4528	0.4399	0.4365	0.4354	0.4352	0.3937	0.1039
130	0.3781	0.3317	0.3217	0.3187	0.3178	0.3176	0.2872	0.0650
140	0.2629	0.2300	0.2234	0.2213	0.2209	0.2208	0.2010	0.0381
150	0.1699	0.1500	0.1466	0.1457	0.1459	0.1459	0.1351	0.0200
160	0.1020	0.0927	0.0919	0.0917	0.0923	0.0923	0.0890	0.0084
170	0.0610	0.0584	0.0593	0.0592	0.0600	0.0602	0.0621	0.0020
180	0.0473	0.0469	0.0484	0.0484	0.0493	0.0495	0.0532	0.0000

Table VI presents the angular distributions for 81-keV photons on the *s* subshells of uranium. These distributions are all closely similar except for  $L_I$ . The variation in the latter can be ascribed to the difference in electron kinetic energy due to the significant binding energy: The  $L_I$  electrons have about 59 keV as against 75 for  $M_I$  and 80 or 81 for the outer subshells. For comparison, the  $L_I$  subshell for 103-keV photons, with electron kinetic energy of about 81 keV, is also presented in Table VI. Its shape is much closer to those of the outer subshells for 81-keV photons than is the  $L_I$  shape for 81-keV photons. This implies that the angular distributions are more sensitive to the electron kinetic energy than to the photon energy. For the heavy element uranium, the Sauter approximation is very inaccurate.

The angular distributions for 81-keV photons on the

*p* subshells of uranium are given in Table VII. The  $p_{1/2}$  subshells have closely similar shapes, as do the  $p_{3/2}$  subshells, with some deviation for the *L* subshells (ascribable again to the binding-energy difference). The  $p_{1/2}$  and  $p_{3/2}$  distributions peak at about the same angle, but the  $p_{3/2}$  shapes are sharper (i.e., dip more in both the forward and backward direction). The Sauter approximation (not presented) fails again in this case.

Table VIII contains the angular distributions for the remaining subshells of uranium for 81-keV photons. The shapes of the  $d_{3/2}$  subshells strongly resemble each other, as do those of the  $d_{5/2}$  subshells. They are not very different from each other, except that the  $d_{5/2}$  distribution dips more in the forward direction. The same comments apply to the  $f_{5/2}$  subshells and the  $f_{7/2}$  subshell.

Generally, then, subshells with the same *l* and *j* have

TABLE VII. Angular distribution of photoelectrons from 81-keV photons on uranium by subshell (*p* states).

$\theta$	$L_{II}$	$M_{II}$	$N_{II}$	$O_{II}$	$P_{II}$	$L_{III}$	$M_{III}$	$N_{III}$	$O_{III}$	$P_{III}$
0	0.5580	0.5222	0.5145	0.5120	0.5124	0.3295	0.3109	0.3102	0.3117	0.3099
10	0.6204	0.5905	0.5844	0.5825	0.5827	0.4731	0.4174	0.4174	0.4187	0.4176
20	0.7695	0.7531	0.7503	0.7499	0.7497	0.6697	0.6634	0.6647	0.6656	0.6652
30	0.9196	0.9153	0.9153	0.9158	0.9154	0.8949	0.8947	0.8962	0.8969	0.8965
40	0.9966	0.9967	0.9969	0.9971	0.9971	0.9973	0.9978	0.9981	0.9983	0.9982
50	0.9746	0.9715	0.9701	0.9693	0.9691	0.9589	0.9562	0.9548	0.9542	0.9544
60	0.8726	0.8629	0.8596	0.8578	0.8575	0.8263	0.8204	0.8180	0.8169	0.8168
70	0.7285	0.7134	0.7090	0.7066	0.7065	0.6596	0.6526	0.6502	0.6493	0.6489
80	0.5770	0.5602	0.5558	0.5533	0.5533	0.5008	0.4953	0.4935	0.4932	0.4930
90	0.4403	0.4257	0.4221	0.4200	0.4200	0.3696	0.3671	0.3663	0.3664	0.3664
100	0.3284	0.3187	0.3166	0.3152	0.3153	0.2697	0.2712	0.2712	0.2715	0.2715
110	0.2429	0.2394	0.2389	0.2384	0.2387	0.1972	0.2031	0.2035	0.2037	0.2039
120	0.1807	0.1839	0.1847	0.1851	0.1853	0.1459	0.1564	0.1567	0.1566	0.1571
130	0.1371	0.1467	0.1488	0.1500	0.1500	0.1102	0.1251	0.1250	0.1240	0.1251
140	0.1074	0.1227	0.1259	0.1282	0.1281	0.0860	0.1045	0.1037	0.1017	0.1031
150	0.0880	0.1079	0.1121	0.1154	0.1153	0.0702	0.0909	0.0896	0.0868	0.0883
160	0.0764	0.0994	0.1041	0.1079	0.1076	0.0609	0.0819	0.0805	0.0776	0.0794
170	0.0704	0.0950	0.0999	0.1036	0.1031	0.0562	0.0765	0.0753	0.0729	0.0754
180	0.0686	0.0936	0.0986	0.1021	0.1016	0.0548	0.0746	0.0735	0.0715	0.0744

TABLE VIII. Angular distribution of photoelectrons from 81-keV photons on uranium by subshell ( $d$  and  $f$  states).

$\theta$	$M_{IV}$	$N_{IV}$	$O_{IV}$	$P_{IV}$	$M_V$	$N_V$	$O_V$	$N_{VI}$	$O_{VI}$	$N_{VII}$
0	0.8413	0.8344	0.8315	0.8289	0.7682	0.7649	0.7635	0.9926	0.9997	0.9353
10	0.8935	0.8882	0.8867	0.8853	0.8376	0.8348	0.8328	0.9999	0.9977	0.9676
20	0.9820	0.9800	0.9802	0.9802	0.9627	0.9612	0.9597	0.9721	0.9528	0.9999
30	0.9864	0.9875	0.9871	0.9868	0.9940	0.9944	0.9947	0.8414	0.8158	0.9258
40	0.8653	0.8682	0.8669	0.8661	0.8752	0.8772	0.8780	0.6248	0.6060	0.7282
50	0.6705	0.6742	0.6735	0.6732	0.6665	0.6692	0.6698	0.4012	0.3908	0.4858
60	0.4744	0.4783	0.4786	0.4788	0.4566	0.4594	0.4602	0.2331	0.2270	0.2835
70	0.3179	0.3216	0.3221	0.3222	0.2951	0.2977	0.2985	0.1326	0.1288	0.1545
80	0.2083	0.2116	0.2121	0.2119	0.1877	0.1899	0.1904	0.0799	0.0776	0.0868
90	0.1376	0.1407	0.1414	0.1413	0.1213	0.1231	0.1235	0.0516	0.0507	0.0544
100	0.0952	0.0983	0.0993	0.0993	0.0821	0.0837	0.0839	0.0356	0.0350	0.0377
110	0.0714	0.0745	0.0756	0.0755	0.0603	0.0618	0.0619	0.0263	0.0255	0.0274
120	0.0585	0.0616	0.0625	0.0623	0.0492	0.0507	0.0506	0.0205	0.0199	0.0204
130	0.0521	0.0548	0.0554	0.0552	0.0438	0.0454	0.0452	0.0167	0.0166	0.0152
140	0.0504	0.0521	0.0517	0.0518	0.0412	0.0431	0.0426	0.0144	0.0146	0.0114
150	0.0520	0.0519	0.0499	0.0501	0.0399	0.0423	0.0416	0.0133	0.0130	0.0091
160	0.0551	0.0526	0.0483	0.0487	0.0395	0.0426	0.0417	0.0127	0.0110	0.0084
170	0.0577	0.0531	0.0468	0.0474	0.0396	0.0434	0.0423	0.0121	0.0093	0.0088
180	0.0586	0.0532	0.0461	0.0468	0.0397	0.0438	0.0426	0.0118	0.0087	0.0091

similar angular distributions. Those with the same  $l$  and different  $j$  peak at about the same angle, the ones with higher  $j$  showing a stronger dip in the forward direction (and to a lesser extent backward). There is much more similarity with the same  $l$  and different  $j$  than vice versa. With increasing  $l$ , the peak of the distribution moves to the forward direction. For a given orbit, the distribution shifts forward with increasing energy. For light elements (such as aluminum), the Sauter approximation gives a satisfactory representation of the shape, though not of the scale; for heavy elements (such as uranium), it is inaccurate. The relative simplicity of the shape and its smooth variation with the relevant variables and quantum

numbers suggest that it might be practical to record the computed angular distributions compactly by fitting them to analytic expressions containing slowly varying parameters.

#### ACKNOWLEDGMENTS

We are indebted to A. Glick and E. C. Imperatore for programming assistance, and to J. T. Waber (Los Alamos Scientific Laboratory) for supplying us with his self-consistent-field output on tape. The uranium computations were performed at the Air Force Weapons Laboratory, where extensive further runs are in progress.